Microwave Intermediate Frequency Equivalent Circuit of GaAs High Electron Mobility Field Effect Transistor Terahertz Detectors

Rahul Yadav*†, Stefan Regensburger*, Andreas Penirschke†, and Sascha Preu*
*Terahertz Devices and Systems
TU Darmstadt, Darmstadt, Germany
Email: (yadav, regensburger, preu)@imp.tu-darmstadt.de
†High Frequency Technology
Mittelhessen University of Applied Sciences, Friedberg, Germany
Email: andreas.penirschke@iem.thm.de

***Abstract*—Field effect transistor (FET) based terahertz rectifiers are promising candidates for sensitive, room-temperature operated high speed (THz) detectors, e.g. in communication, medical, biochemical, security, quality control applications, or beam diagnostic applications at particle accelerators. This paper investigates the equivalent circuit in the intermediate frequency band from 0.1 to 65 GHz with S-parameter measurements in order to enable implementation with high speed post detection electronics. Preliminary results are obtained by de-embedding On-Wafer measurements and compared with theoretical expectations from hall measurements and a simplified equivalent circuit. The knowledge of the channel behavior and impedance is mandatory for impedance matching to IF circuitry in advanced detector designs.**

***Index Terms*—Coplanar Waveguides (CPW), De-embedding, Field Effect Transistor (FET), Terahertz (THz) detectors, Two Dimensional Electron Gas (2DEG)**

I. Introduction

Field effect transistor (FET)-based rectifiers became excellent Terahertz detectors at room temperature with noise-equivalent powers in the pW/$\sqrt{Hz}$ range using antenna-coupled versions [1]. In most cases, the DC current generated by FETs upon irradiation with THz signals is measured (detected). In many cases, the lock-in technique is applied using modulation frequencies in the kHz range for the noise reduction. For communication applications as well as for beam diagnosis at accelerator facilities [2], however, IF frequencies in the tens of GHz range are required. The intrinsic speed (transit-time cut-off frequency, e.g.) of GaAs High electron mobility transistors (HEMTs) indeed permits such high IF frequencies. In order to embed the FET in adequate post-processing IF circuitry, a decent understanding of the IF impedance is mandatory. Therefore, this work is focused on the IF performance of FETs, its two dimensional electron gas (2DEG) channel and ungated areas at 0.1-65 GHz using S-parameter measurements. We further use a theoretical equivalent circuit model from [3] where the parameters of the circuit elements were derived from Hall data and compare it to experimental data. The precise de-embedding of the measured data is performed using Thru (T), Line (L), Reflect (L) de-embedding techniques for extraction of R_{2DEG}, L_{2DEG} and C_{2DEG} values of 2DEG.

We are thankful for cooperation between TU Darmstadt, Darmstadt, Germany and Mittelhessen University of Applied Sciences, Friedberg (Hesse), Germany for this project.

II. Theory

The high electron mobility in GaAs/AlGaAs HEMTs is achieved by remote doping within the barrier which supplies the charges for the 2DEG channel. The material of the channel is intrinsic GaAs with high mobility that is not obscured by scattering with donor atoms. For the devices investigated in this work, the 2DEG channel is located 30 nm below the surface of the substrate as shown in Fig. 1(a). The band diagram is shown in Fig. 1(b). There are two kinds of rectification processes in FET detectors: At frequencies below its cut-off frequency, resistive mixing is achieved by synchronously coupling an AC signal to the GS and the DS port. At higher frequencies, plasmonic mixing persists far beyond f_T and f_{max} [4]. Equations (1)-(4) show the simplified version of resistive mixing in the channel.

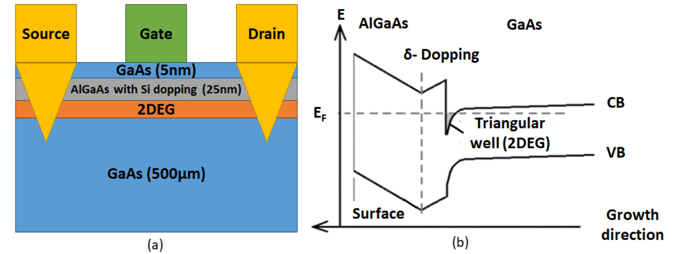

Fig. 1. (a) Block diagram of the HEMT sample. (b) Band diagram of the HEMT. [4]

978-1-7281-8439-5/21/$31.00 © 2021 IEEE

© 2021 IEEE. Personal use of this material is permitted. Permission from IEEE must be obtained for all other uses, in any current or future media, including reprinting/republishing this material for advertising or promotional purposes, creating new collective works, for resale or redistribution to servers or lists, or reuse of any copyrighted component of this work in other works.

$$n^{(2D)} \sim U_G(t) \sim U_{THz}(t) \quad (1)$$

$$v \sim U_{DS}(t) \sim U_{THz}(t), \quad (2)$$

where v is the electron drift velocity, $n^{(2D)}$ is the 2D electron density, $U_G(t)$ is electric potential provided at gate terminal (gate bias), $U_{DS}(t)$ is the electric potential across the drain and source terminal, $U_{THz}(t)$ is the THz bias coupled synchronously to gate and drain. The electrical current density is given by

$$j = en^{(2D)}(t)v(t) \sim [U_{THz}(t)]^2 \quad (3)$$

$$j = [U_{THz}(t)]^2(1 + \cos(2\omega_{(THz)}t)) \quad (4)$$

The first term in Equation (4) is the rectified current. As $j \sim {U_{THz}}^2 \sim P_{THz}$, the detector is a direct power detector. Phenomenologically, the detection process of the plasmonic rectification mechanism is similar to resistive mixing, however, the channel cannot be considered as a lumped element any more. Plasma waves may spread into the channel and be rectified during propagation. The theory of THz detection using FETs is explained in [4] and [5].

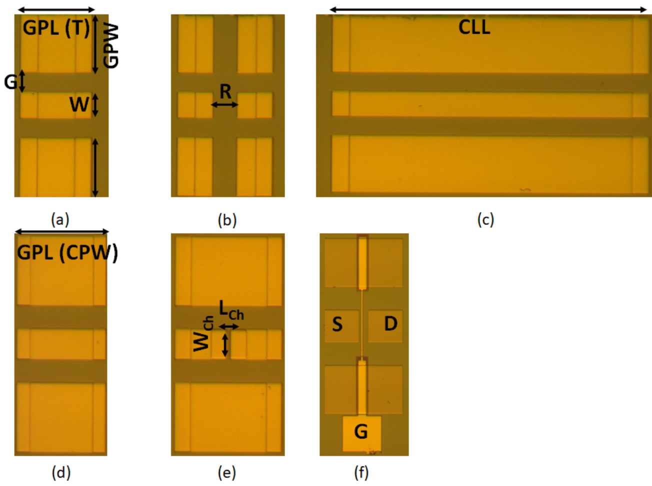

Fig. 2. (a) Thru structure (G: Gap between signal and ground plane, W: Width of the inner conductor, GPW: Ground plane width, GPL(T): Ground plane length for Thru). (b) Reflect structure (R: Distance between two reflect structures). (c) Line structure (CLL: Calibration line for 0.1 to 65 GHz). (d) CPW for reference (GPL(CPW): Ground plane length for reference structure). (e) Only 2DEG structure (L_{Ch}: Channel length, W_{Ch}: Channel width). (f) FET structure (S: Source, D: Drain, G: Gate)

For the On-Wafer measurements, probes are brought in contact at the end of the transmission line (defining the measurement plane) but not directly at the device plane (FET in our case). Therefore de-embedding of the measured S-parameters is required to shift the calibration plane to the device plane. In this study, Thru, Reflect and Line technique (TRL) is used for de-embedding the measured S-parameters. Fabricated Thru, Reflect and Line structures are shown in Fig. 2(a), (b) and (c), respectively. There are three different kinds of structures: Coplanar Waveguide (CPW) for reference (Fig. 2(d)), an ungated device (Fig. 2(e)) and a CPW coupled FET

TABLE I
STRUCTURES FABRICATION PARAMETERS

Abbreviations	***Dimensions(μm)***
GPL (T)	150
GPL (CPW)	250
GPW	150
W	66
G	50
R	50
CLL	517
W_{Ch}	60 and 66
L_{Ch}	2, 10 and 25

device (Fig. 2(f)). The dimensions of the fabricated structures are shown in Table 1. The devices were fabricated in house using UV photo-lithography. On-wafer VNA measurements

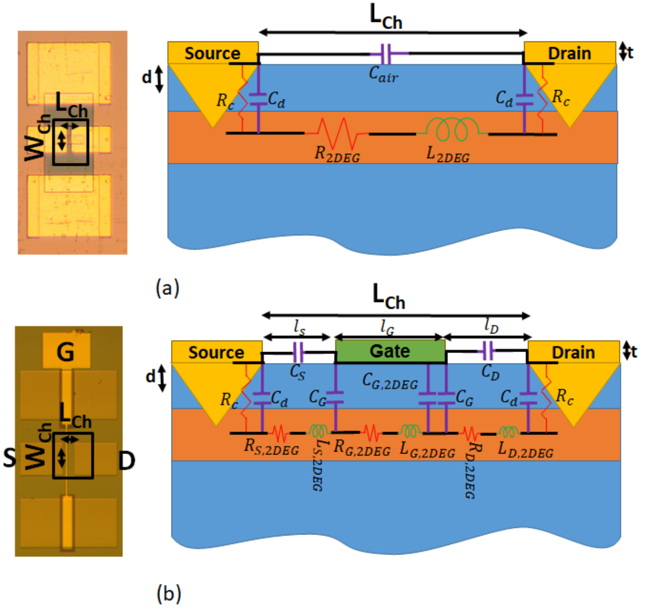

Fig. 3. (a) Left: Ungated 2DEG structure, top view; Right: Side view of the center signal strip of CPW with lumped elements circuit (L_{Ch}: Channel length, W_{Ch}: Channel width, d: Distance of 2DEG from surface of wafer (30 nm), t: Thickness of metal layer, R_c: Contact resistance, C_d: Capacitance due to depth of 2DEG, C_{air}:Capacitance in air, R_{2DEG}: Total resistance of the 2DEG, L_{2DEG}: Total inductance of 2DEG).(b) Left: Fabricated FET structure, top view; Right: Side view of the FET structure with lumped element circuit components (l_S: Length of ungated channel towards source side, l_G: Length of gated channel, l_D: Length of ungated channel towards drain side, C_S: Capacitance in air on ungated channel towards source side, C_D: Capacitance in air on ungated channel towards drain side, $R_{S,2DEG}$:Resistance of ungated channel towards source side, $R_{D,2DEG}$:Resistance of ungated channel towards drain side, $R_{G,2DEG}$: Resistance of the gated channel, $L_{S,2DEG}$:Inductance of ungated channel towards source side, $L_{G,2DEG}$:Inductance of the gated channel, $L_{D,2DEG}$: Inductance of the ungated channel towards drain side, $C_{G,2DEG}$: Capacitance of the gated channel area, C_G: Stray capacitance at the ends of the gate)

were performed using a cascade microtech system. Infinite GSG probes of 150 μm pitch were used for measurement from 0.1 to 65 GHz. Calibration at the probe tips was done using standard SOLT (Short, Open, Load, Thru) technique

on a ceramic substrate followed by TRL de-embedding using structures on the fabricated GaAs chip. The de-embedding was performed during data analysis using MATLAB.

Refs. [3], [6] and [7] show a general equivalent circuit diagram for the transistor channel with various ways to calculate the channel parameters that are later used to compare to measured data. The equivalent circuit diagram for de-embedding used in this paper is shown in Fig. 3. We investigate two cases: Fig. 3(a) shows the diagram and parameter definition for an ungated device, which consists of only source and drain contacts but no gate contact. This case allows to extract circuit parameters for the undesired, but usually present ungated channel length between the gate and the drain contact in HEMTs. Fig. 3(b) shows the diagram for the gated device including both gated and ungated areas. For the ungated section of the device, the resistance of 2DEG channel is given by [3] and [6]

$$R_{2DEG} = r_0 \cdot L_{Ch} \tag{5}$$

where L_{Ch} is the channel length and r_0 is resistance per unit length of the 2DEG. The inductance of the channel is given by

$$L_{2DEG} = l_0 \cdot L_{Ch} \tag{6}$$

where l_0 is inductance per unit length of the 2DEG. For simplicity, we assumed that the metallization of the channel does not noticeably or only slightly alter the charge concentration in the channel which is experimentally supported in [3]. Therefore, the R_{2DEG} and L_{2DEG} for the FET can be calculated as

$$R_{i,2DEG} = r_0 \cdot l_i \tag{7}$$

$$L_{i,2DEG} = l_0 \cdot l_i \tag{8}$$

where l_i is the length and $i = D,\ S\ or\ G$. The $C_{G,2DEG}$ is calculated as

$$C_{G,2DEG} = c_0 \cdot l_G \tag{9}$$

where c_0 is the capacitance per unit length of 2DEG.

The signal flow graph of the CPW structure used for reference is shown in Fig. 4(a) Two contact pads are shown where the probe tips get in contact by C_{PA} (left side in yellow colour) and C_{PB} (violet colour on right side). The red part in center depicts the transmission line (analogous to Fig. 2(d)). The FET is shown in Fig. 4(b), where the active part is shown with green colours, coupled to the transmission lines T_{xlineA} and T_{xlineB} on both sides (shown in red colour).

De-embedding was performed following the ten terms equation to find the unknown parameters as explained very well in [8], based on transmission line theory [9]. Measured S-parameters from Thru, Reflect and Line structures (Fig. 2(a, b and c) respectively) are applied to find the values of the contact pads as proposed in [8]. The determined contact pad parameters can now be used to de-embed the S-parameters on

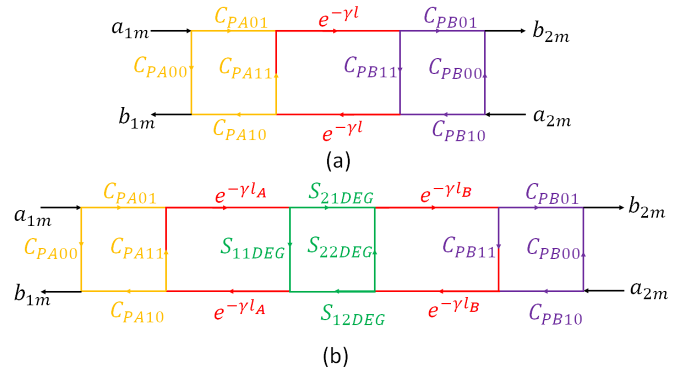

Fig. 4. (a) Signal flow graph for only CPW structure (a_{1m}:Incident wave at port 1, a_{2m}:Incident wave at port 2, b_{1m}: Reflected wave at port 1, b_{2m}: Reflected wave at port 2). (b) Signal flow graph for the FET structure (l_A: Length of transmission line A (left side), l_B: Length of transmission line B (right side))

CPW reference structure (Fig. 2(d)). The propagation constant γ and characteristic impedance Z_c is calculated as

$$e^{-\gamma l} = \frac{(1 - S_{11txline}^2 + S_{21txline}^2)}{2 \cdot S_{11txline}} \pm \sqrt{\frac{(S_{11txline}^2 - S_{21txline}^2 + 1) - 4 \cdot S_{11txline}^2}{2 \cdot S_{21txline}^2}} \tag{10}$$

$$Z_c = Z_0 \cdot \sqrt{\frac{(1 + S_{11txline})^2 - S_{21txline}^2}{(1 - S_{11txline})^2 - S_{21txline}^2}} \tag{11}$$

where $S_{11txline}$ and $S_{21txline}$ are de-embedded S-parameters of CPW reference structure, $txline$ stands for CPW transmission line and l is the length of the transmission line. Using the obtained propagation constant γ, calculation of $e^{-\gamma l_A}$ and $e^{-\gamma l_B}$ is possible where l_A and l_B are two transmission line lengths on the left and right side of the gated 2DEG, respectively (as shown in Fig. 4(b)). The transmission matrix T is defined by incident and reflect waves in order to evaluate the cascaded network, commonly referred to as wave cascade matrix (WCM). Parameters of the 2DEG channel were extracted using the WCM concept. For the transmission lines A and B, the WCMs are found as follows:

$$[T]_{TxlineA} = \begin{bmatrix} \cosh(\gamma \cdot l_A) & Z_c \cdot \sinh(\gamma \cdot l_A) \\ \frac{\sinh(\gamma \cdot l_A)}{Z_c} & \cosh(\gamma \cdot l_A) \end{bmatrix} \tag{12}$$

$$[T]_{TxlineB} = \begin{bmatrix} \cosh(\gamma \cdot l_B) & Z_c \cdot \sinh(\gamma \cdot l_B) \\ \frac{\sinh(\gamma \cdot l_B)}{Z_c} & \cosh(\gamma \cdot l_B) \end{bmatrix} \tag{13}$$

By using the cascade network concept,

$$[T]_M = [T]_{CPA} \cdot [T]_{TxlineA} \cdot [T]_{2DEG} \cdot [T]_{TxlineB} \cdot [T]_{CPB}, \tag{14}$$

where $[T]_M$ are T-parameters of measured S-parameters, $[T]_{CPA}$ of contact pad A, $[T]_{CPB}$ for contact pad B, $[T]_{TxlineA}$ of transmission line A, $[T]_{TxlineB}$ of transmission line B and $[T]_{2DEG}$ of 2DEG channel need to be found.

$$[T]_{2DEG} = [T]_{TxlineA}^{-1} \cdot [T]_{CPA}^{-1} \cdot [T]_M \cdot [T]_{CPB}^{-1} \cdot [T]_{TxlineB}^{-1} \tag{15}$$

$$[T]_{2DEG} = \begin{bmatrix} T_{11,2DEG} & T_{12,2DEG} \\ T_{21,2DEG} & T_{22,2DEG} \end{bmatrix} \quad (16)$$

The obtained T-parameters for 2DEG can be converted to S-parameters

$$[S]_{2DEG} = \begin{bmatrix} S_{11,2DEG} & S_{12,2DEG} \\ S_{21,2DEG} & S_{22,2DEG} \end{bmatrix} \quad (17)$$

The extracted S-parameters of the ungated 2DEG or FET are used to determine values of lumped elements of the 2DEG equivalent circuit.

III. Results and Discussions

Fig. 5 (top left and right) shows a comparison between simulation and measured S-parameters for the Thru structure. The reflection coefficient S_{11} deviates by around 10 dB. More oscillations are present at lower frequencies and converge towards higher frequencies. This is probably due to presence of standing waves. We remark that the S_{11} and S_{22} parameters are about 30 dB smaller than the S_{12} and S_{21} such that minor perturbations of the transmission parameters can already cause this discrepancy. A consequence of this is seen clearly when parameters of the contact pads are calculated (e.g. in Fig. 5 middle left graph). While the deviation of the reflection coefficient is large, the transmission coefficient S_{21} only deviates by 0.275 dB and also excellently agrees with the simulation. After using the TRL de-embedding technique, reflection and transmission coefficients of contact pads A and B are extracted, which are shown in Fig. 5 (middle row). The transmission coefficients of contact pads A and B are the same in amplitude but opposite in sign or mirror images. This is a novel result which as per the authors knowledge has not been seen in previous papers on de-embedding. The characteristic impedance of CPW structure is quite well related (deviation of $<1\ \Omega$) for calculated and simulated results as shown in Fig. 5 (bottom left). The de-embedding of CPW structure used as a reference is shown in Fig 5 (bottom right). It has been observed that the reflection coefficient is approximately 80 dB after de-embedding compared to 30 dB before de-embedding. This means, most of the signal is getting reflected from the contact pads A and B. Also oscillations observed for measured S_{11} are smaller after de-embedding which means the standing waves are dominant on the transmission line. For the transmission coefficients, 0.3 dB of deviation is observed comparing before and after de-embedding.

With the help of extracted values of contact pads A and B, S-parameters at the 2DEG plane have been extracted by the WCM method. The values of r_0 and l_0 can be extracted from the S-parameters at the 2DEG plane and the equivalent circuit diagram of the ungated 2DEG structure as shown in Fig. 3(a).

$$Z_{2DEG} = Z_0 \cdot \sqrt{\frac{(1+S_{11,2DEG})^2 - S_{21,2DEG}^2}{(1-S_{11,2DEG})^2 - S_{21,2DEG}^2}} \quad (18)$$

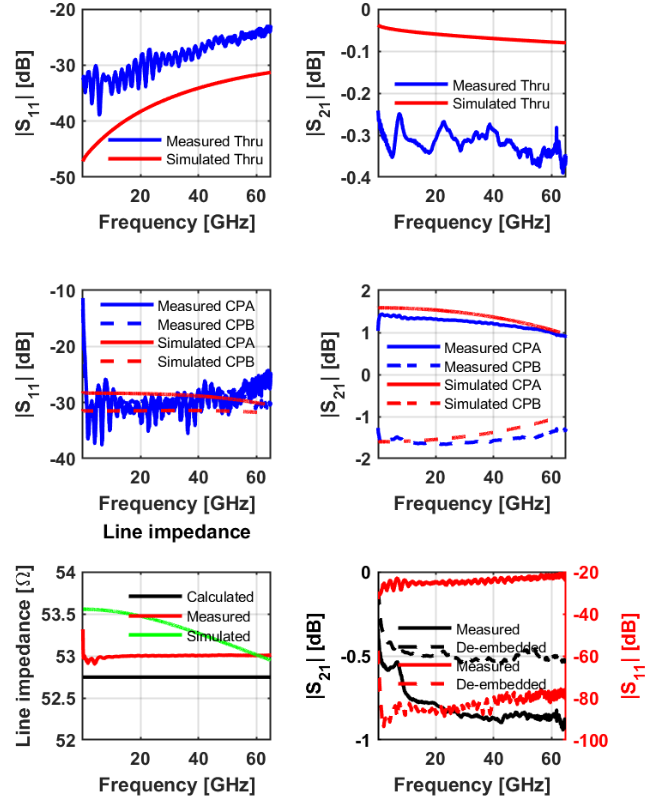

Fig. 5. Top: Simulated and measured reflection and transmission coefficients for Thru structure; Middle: Simulated and measured reflection and transmission coefficients for contact pads A and B [10]; Bottom (left): Calculated, simulated and measured characteristic impedance of CPW; Bottom (right): Measured and de-embedded reflection and transmission coefficients of CPW

Using the Hall measurement data, the lumped element parameters of the ungated and gated 2DEG can be derived as [3]

$$r_0 = \frac{1}{q_e \cdot \mu \cdot W_{Ch} \cdot n^{(2D)}} \quad (19)$$

$$l_0 = \frac{m^*}{q_e^2 \cdot W_{Ch} \cdot n^{(2D)}} \quad (20)$$

$$c_0 = \frac{\epsilon_0 \cdot \epsilon_r \cdot W_{Ch}}{d} \quad (21)$$

where, r_0 is the resistance per unit length of channel, l_0 is the inductance per unit length of channel, c_0 is the capacitance per unit length of channel, q_e is the charge of an electron, μ is the electron mobility in GaAs, $n^{(2D)}$ is the sheet electron density, W_{Ch} is the channel width, d is the distance of the 2DEG from wafer surface/gate metal, ϵ_0 is the permittivity of free space, $\epsilon_r \approx 13$ is the relative permittivity of GaAs, $m^* = 0.067 m_0$ is the effective electron mass in GaAs. The calculated values are shown in Table II.

Using de-embedded S-parameters, r_0 and l_0 are obtained from the ungated 2DEG as shown in Fig. 6 for two different

TABLE II
DATA FROM HALL MEASUREMENT

Parameters	W_{Ch} ***60*** μm	W_{Ch} ***66*** μm
Mobility (μ)	5990 cm^2/vs	5990 cm^2/vs
Sheet electron density($n^{(2D)}$)	4.57 e^{11} $1/cm^2$	4.57 e^{11} $1/cm^2$
r_0	3.81 e^7 Ω/m	3.46 e^7 Ω/m
l_0	8.69 e^{-6} H/m	7.94 e^{-6} H/m
c_0	2.30 e^{-7} F/m	2.53 e^{-7} F/m

channel lengths (L_{Ch}=2 μm and 10 μm) but same channel width (W_{Ch}=60 μm). In Fig. 6 left, r_0 is $\approx 15-20\%$ off from the expected value (as per Hall measurement). This is still an excellent agreement since the Hall measurement is performed on wafer without any structures. During fabrication, the metal deposition and fabrication techniques modify the semiconductor surface which has a direct impact on the carrier concentration in the channel. In [3] we found a change on a similar scale as found here. Above 40 GHz, a slight decay is observed which can be explained due to the presence of a stray capacitance in the system, which can also be seen in right graph for l_0. The channel inductance per length l_0 shows a decent match to the expected value from the Hall data.

The r_0, l_0, and c_0 values for a channel length (L_{Ch}) of 25 μm and a channel width (W_{Ch}) of 66 μm are shown in Fig. 7. Two different gate positions are considered: (i) center of the channel (Gate symmetric) and (ii) close to source contact (Gate placed asymmetrically). The r_0, l_0 and c_0 values are almost the same for both cases. Here r_0 shows $\approx 20\%$ decay from lower to higher frequencies. This is again a sign of an unknown stray capacitance. Alternatively, it may be due to the fact that gated and ungated areas have slightly different r_0 and l_0 which was neglected in this work. A similar trend is seen for l_0 and c_0. The de-embedded channel impedance (Fig. 7 bottom right) decreases less quickly than expected towards high frequencies.

IV. CONCLUSION

Precise de-embedding of a FET has been performed for transmission line coupled structures. TRL de-embedding and extraction of the contact pad parameters shows that most of

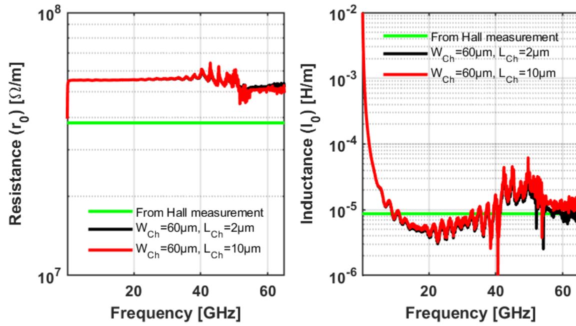

Fig. 6. Left: Resistance per unit length; Right: Inductance per unit length for ungated 2DEG structure

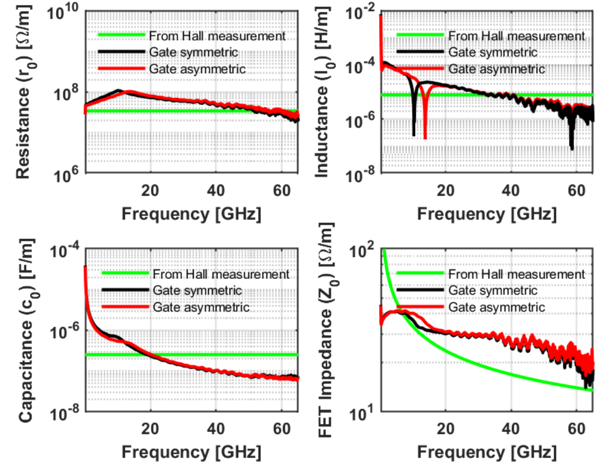

Fig. 7. Top (Left):Resistance per unit length of FET; Top (Right): Inductance per unit length of FET; Bottom (Left): Capacitance per unit length of FET; Bottom (Right): Impedance of FET

the reflection is at the entry ports, while the transmission loss is 0.5 dB compared to measured and de-embedded for CPW structures. The results are in very good agreement to the values derived from Hall results using a theoretical model. However, there is an unexpected decay of r_0 and l_0 towards higher frequencies of the investigated frequency range from 0.1 to 65 GHz. A plausible explanation may be a difference in the r_0 and l_0 values for gated and ungated areas that has been neglected in this work. Still, the expected FET impedance is sufficiently well understood and confirmed by experiments to allow for approximate impedance matching to high speed post detection electronics.

ACKNOWLEDGMENT

We would like to thank Mr. Amlan Kusum Mukherjee for active discussion on the topic. Also we are grateful to the Hesse ministry of science and culture (HMWK) for funding the position of Mr. Rahul Yadav.

REFERENCES

[1] U. R. Pfeiffer, J. Grzyb, H. Sherry, A. Cathelin and A. Kaiser,"Toward low-NEP room-temperature THz MOSFET direct detectors in CMOS technology,", presented at the *38thInternational Conference on Infrared, Millimeter, and Terahertz Waves (IRMMW-THz),* Mainz, Germany, 2013, pp. 1-2. DOI:10.1109/IRMMW-THz.2013.6665522

[2] S. Regensburger, S. Winnerl, J. M. Klopf, H. Lu, A. C. Gossard and S. Preu,"Picosecond-Scale Terahertz Pulse Characterization With Field-Effect Transistors," in *IEEE Transactions on Terahertz Science and Technology,* vol.9, no. 3, pp. 262-271, May 2019, DOI:10.1109/TTHZ.2019.2903630

[3] S. Regensburger, A.K.Mukherjee, S.Schönhuber, M.A.Kainz, S.Winnerl, J. M. Klopf, H.Lu, A.C.Gossard, K.Unterrainer and S.Preu,"Broadband Terahertz Detection With Zero-Bias Field-Effect Transistors Between 100 GHz and 11.8 THz With a Noise Equivalent Power of 250 pW/$\sqrt{\text{Hz}}$ at 0.6 THz," in *IEEE Transactions on Terahertz Science and Technology,* vol.8, no. 4, pp.465-471, July 2018, DOI:10.1109/TTHZ.2018.2843535

[4] S.Preu,S.Kim, R.Verma, P.G.Burke,M.S. Sherwin, and A.C.Gossard,"An improved model for non-resonant terahertz detection in field-effect transistors ," in *Journal of Applied Physics,* vol. 111, no. 2, pp. 024502, Jan. 19, 2012, DOI:10.1063/1.3676211

[5] M.Dyakonov and M. Shur,"Shallow water analogy for a ballistic field effect transistor: New mechanism of plasma wave generation by dc current," in *Phys. Rev. Lett.,* vol. 71, no. 15 pp. 2465-2468, Oct. 1993, DOI:10.1103/PhysRevLett.71.2465

[6] I.Khmyrova and Yu.Seijyou,"Analysis of plasma oscillations in high-electron mobility transistorlike structures: Distributed circuit approach," in *Applied Physics Letters,* vol. 91, no. 14 pp. 143515, 2007, DOI:10.1063/1.2794772

[7] I.Khmyrova,"Equivalent circuit modeling of terahertz devices and resonant MEMS with two-dimensional electron gas system,", presented at the *15th IEEE Mediterranean Electrotechnical Conference,* Valleta, Malta, 2010.,pp. 1027-1032,DOI:10.1109/MELCON.2010.5475905

[8] G.Tang, H.Yao, X.Ma, Z.Jin and Xinyu Liu,"On-wafer de-embedding techniques from 0.1 to 110 GHz ," in *Journal of Semiconductors,* vol. 36, no. 5, pp. 054012, May, 2015, DOI:10.1088/1674-4926/36/5/054012

[9] D. M. Pozar, "Microwave engineering," in *Transmission line theory,* 3rd ed., John Wiley-Sons, Inc., New Jersey, NJ, USA, 2005, pp. 49–84.

[10] R.Yadav, S.Regensburger, A.Penirschke and S.Preu,"Optimization of GaAs Based Field Effect Transistors for THz Detection at Particle Accelerators", presented at the *9th International Beam Instrumentation Conference,* Santos, Brazil, Sep. 14-18, 2020.